

Article

Reconstruction of Seasonal Net Erosion in a Mediterranean Landscape (Alento River Basin, Southern Italy) over the Past Five Decades

Nazzareno Diodato ¹ and Gianni Bellocchi ^{1,2,*}

¹ Met European Research Observatory-International Affiliates Program of the University Corporation for Atmospheric Research, 82100 Benevento, Italy; scodalabdiodato@gmail.com

² UCA, INRA, VetAgro Sup, Unité Mixte de Recherche sur Écosystème Prairial (UREP), 63000 Clermont-Ferrand, France

* Correspondence: gianni.bellocchi@inra.fr; Tel.: +33-4-4376-1601

Received: 28 August 2019; Accepted: 31 October 2019; Published: 4 November 2019



Abstract: In the low Mediterranean basin, late spring and autumn rainfall events have the potential to increase discharge and transport substantial amounts of sediment soil (that is, the net soil erosion from a watershed). For the Alento River Basin (ARB), located in the low Tyrrhenian coast of Italy, we estimated changes of net erosion as dependent on the seasonality of antecedent soil moisture and its control on rainfall-runoff and erosivity. Based on rainfall and runoff erosivity sub-models, we developed a simplified model to evaluate basin-wide sediment yields on a monthly basis by upscaling point rainfall input. For the period 1951–2018, the reconstruction of a time series of monthly net erosion data indicated a decreasing trend of the sediment yield after 1991. Revegetation and land abandonment that occurred in the last decades can explain such a decrease of net erosion, which occurred even when rainfall erosivity increased. This response, obtained at the basic scale, does not exclude that rapidly developing mesoscale convective systems, typically responsible for the heaviest and most destructive rainfall events in the ARB, can affect small catchments, which are the most vulnerable systems to storm-driven flash floods and soil erosion hazards during soil tilling in spring and at beginning of autumn.

Keywords: erosive rainfall; parsimonious modeling; river basin; soil erosion

1. Introduction

Environmental changes are a prominent topic for Earth and environmental sciences, but its importance increases during crucial changes and different types of climate extremes that potentially lead to crises of some kind [1,2]. Extreme climate events are often associated with land degradation [3,4]. Soil erosion, in particular, is a pervasive form of soil degradation and a matter of increasing concern because of its implications for food security with the rapidly increasing world population [5]. Modeling processes that produce geomorphological hazards require understanding of how landscape components respond to forced conditions of land use change and to the climatic regime [6,7]. This is valuable to inform the assessment of future planning [8,9], but soil erosion monitoring systems tracking downstream sediment movement may be costly, and require focused efforts to manage land and water resources [10]. Because of this cost, modeling is playing an increasingly significant role [11]. This applies to the quantification of sediment dynamics, which is key to Earth-system science as documented in geology [12], biogeochemistry [13], and human activities [14]. It is also key to advancing our quantitative understanding and predictive capabilities of regional and sub-regional sediment fluxes. In the last decade, for instance, some geomorphological studies of long-term scale have affected the

coastal areas of Southern Italy [15,16], which is the focus of this study, but research is still needed, given the differences in the responses at monthly and annual scales. Especially in mountainous agricultural areas, hydro-geomorphological degradation processes represent a complex issue, which manifests in a variety of phenomena [17]. Widespread modeling approaches are crucial in assessing climate variability and land cover [18,19], two important factors affecting the environmental sustainability of landscape systems [20–22]. The latter are dynamic and sensitive, and highly controlled by a set complex of climatic, geomorphic, and ecologic processes [23]. Sediment rates may be expected to change in response to changes in climate for a variety of reasons, responding both to the total amount of rainfall and to differences in rainfall intensity. However, the dominant variables appear to be rainfall intensity and energy, rather than rainfall amount alone. Nearing et al. [24] predicted that for every 1% increase in total rainfall, erosion rate would increase by only 0.85% if there was no corresponding increase in rainfall intensity. If both rainfall amount and intensity were to change together in a statistically representative manner, erosion rate would increase by 1.7% for every 1% increase in total rainfall, according to Pruski and Nearing [25]. Despite advances made in recent years, local-to-global modeling of sediment fluxes remains a research challenge [26]. For instance, numerical models have limitations for predicting basin sediment yield [27], especially over long timescales, and require access to powerful computer resources [28]. Their evaluation is also difficult because of the scarcity of measurements [29].

To deal with these issues, we propose an integrative methodology, based on the concepts of Foster et al. [30] and adapted from Thornes' [31] model (NETAM: Net Erosion Thornes-Adapted Model), offering a parsimonious interpretation of the relationship between hydrological data and basin-wide net erosion. We refer here to soil erosion by water, i.e., the result of rain detaching and transporting soil, either directly by means of rain splash or indirectly by rill and gully erosion. The capability to reproduce at basin scale the combined effects of hydro-climatological processes, including sediment transport, in the absence of distributed spatial and temporal data, relies on representation of the drainage basin as a homogeneous landform unit. In this way, the NETAM approach upscales point rainfall input data to area units where hydrological processes respond. This results in a long series of rainfall data from a single station (1951–2018 for the Alento River Basin (ARB)) that is a sufficient input for the parsimonious model. The use of a NETAM time-series model is thus motivated by its potential for capturing the significant and changing environment (including climate, vegetation cover, and erosive-resistance climate changes) with easily available data. Its evaluation in the ARB offers a unique opportunity to explore geomorphological processes in this Mediterranean fluvial basin.

2. Study Area

The Alento River Basin (ARB) is located between the Cilento, Vallo di Diano and Alburni National Park (Campania, southern Apennine), which is one of the largest Italian National Parks, stretching between 40°00' and 40°30' N, and 14°50' and 15°00' E (Figure 1a,b), with a total area of 428 km². The main weather station is located in Gioi Cilento (40°17' N, 15°13' E), which holds the longest and most reliable hydrological data of the basin area (Figure 1c).

Altitudes range from sea level to Mt. Cervati (1898 m a.s.l.). Other peaks are located in the easternmost portion of the basin with Mount Sacro (1705 m a.s.l.), Mount Scuro (1610 m a.s.l.), and Mount Falascoso (1494 m a.s.l.). In southern Campania Region, three bioclimatic zones are present: The Mediterranean flat-hills along the coast, the pre-Apennines area, and inner hilly-mountainous zones. Precipitations vary from 600 to 1800 mm year⁻¹, depending on altitude and distance to sea (Figure 2a). The highest precipitation falls on Picentini Mountains, to the north, and Campano-Lucano Apennine, to the south (Figure 2a). With an enlarged view (Figure 2b), we can detect more resolute spatial variability also across the ARB. Here, precipitation varies from 800 mm year⁻¹ on the valley to 1400 mm year⁻¹ on the mountains of the National Park.

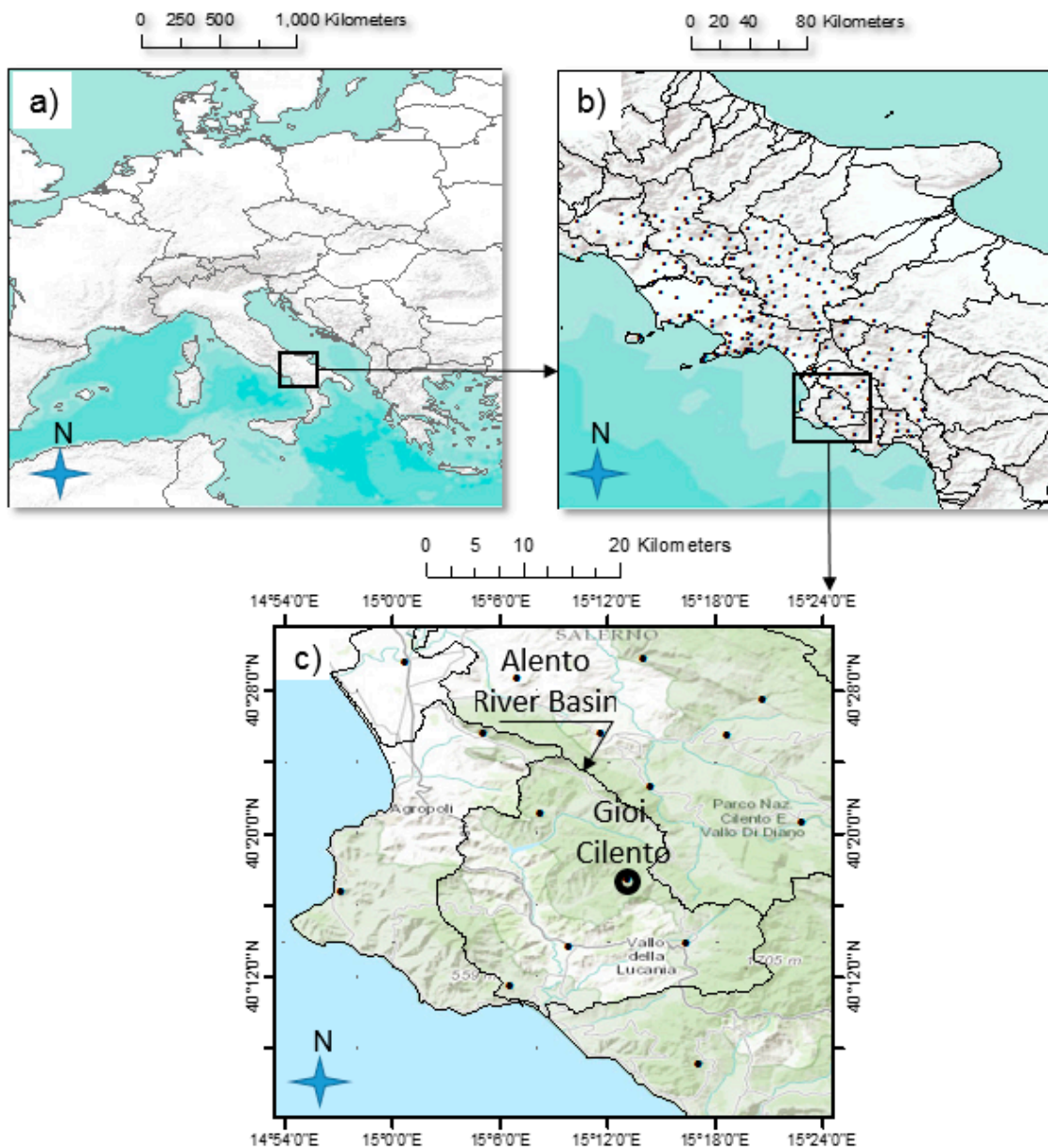


Figure 1. (a,b) Location maps of the Alento River Basin (ARB), and (c) hydrological data of the basin area. The station of Gioi Cilento (big dot) was used for the pluviometric elaboration and model-derived variables. All other stations (small dots) were used for mapping the annual mean precipitation and erosivity over the period 1951–2000.

River morphology is complex in the study region. The upstream part of the basin presents a narrow alluvial valley with steep slopes. Downstream, however, the river makes a turn towards the south. Subsequently, the river assumes a braided configuration down until the reservoir of Piano della Rocca, in the commune of Prignano Cilento ($40^{\circ}20' N$, $15^{\circ}04' E$). Further downstream, the river mostly takes a meandering character. The geological nature of the rocks is dominated by the “Flysch of the Cilento” (i.e., limestone and silicoclastic substrata), wherein the main river basins (Alento, Calore, Mingardo, Bussento) are established [32]. Overall, the basin area is not prone to gully erosion, as it is dominated by erosion-resistant lithologies. With the only exception of the far northern/north-eastern part of the catchment, which is characterized by the presence of limestones pertaining to the Apennine Chain, these formations are quite homogeneous in hydrogeological terms and may be merged into a single hydrogeological complex of arenaceous–marly–clayey formation, which is relatively poorly permeable.

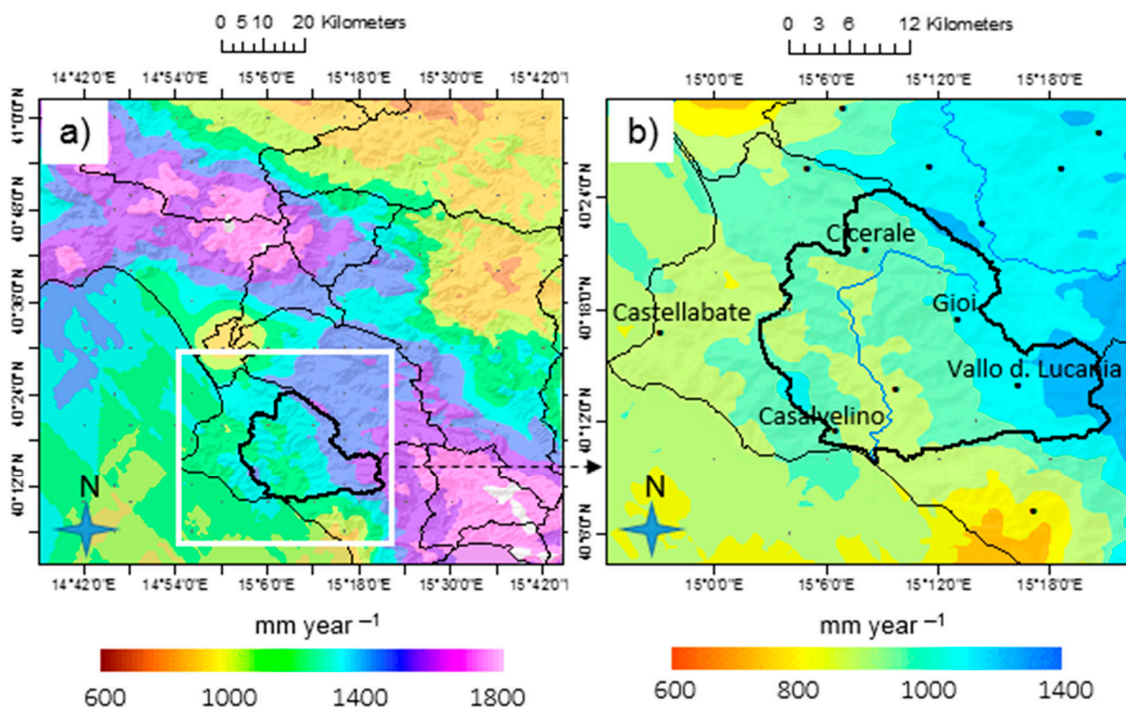


Figure 2. (a) Annual mean precipitation map over southern Campania Region and (b) relative zoom for the Alento River Basin upon the period 1951–2000. The maps were produced with ESRI-ArcGIS via Geostatistical Analyst (Lognormal Detrended Ordinary Cokriging with altitudinal covariate used for the purpose).

3. Materials and Methods

3.1. Data Collection

Daily rainfall data for the period 1951–2000 were collected from the rain gauge network of the *Servizio Idrografico and Mareografico Nazionale* (SIMN, National Hydrographic and Marine Service) [33], nowadays *Rete Mareografica Nazionale* (National Tidegauge Network, <http://www.mareografico.it>), continued by *Centro Funzionale Multirischi Protezione Civile della Regione Campania* (Multirisk Functional Centre of Civil Protection–Campania Region, <http://centrofunzionale.regione.campania.it/#/pages/dashboard>). However, for sediment data, only a long-term (1951–2000) average value was available [34]. Under this limited calibration condition, credibility of final output estimates was founded on the sub-model validation. The model was thus calibrated against long-term average net erosion and then validated for its erosivity and runoff sub-models, using monthly-aggregated data, as determined in the ARB from the sub-periods 2002–2008 (RUSLE-based erosivity at Gioi Cilento [35]) and 1958–1973 (SIMN measurements at the outlet of the ARB), respectively.

Monthly vegetation cover fraction was assessed with Normalized Difference Vegetation Index (NDVI) data, as derived from the GIMMS–KNMI Climate Explorer platform (<http://climexp.knmi.nl>), and rearranged to characterize the inter-annual evolution [16]. Olive orchards and sclerophyllous Mediterranean vegetation prevail along the coast, whereas forest landscape is dominant in the inner area, mainly represented by *Quercus cerris* or *Fagus sylvatica* woods. Not negligible is also the presence of riparian forest cover, dominated by *Salix alba*, *Populus nigra*, *Populus alba*, and *Alnus glutinosa*. Smallholder agriculture (arable land and orchards) dominates, sustained by mechanization, road infrastructure, availability of groundwater stocks, and water storage for irrigation purposes.

3.2. Net Erosion Model

Net soil water erosion is a measure of average sediment yield (soil net erosion) occurring basin-wide over time (Figure 3a), resulting from the sum of the sediment produced by all erosional sources, including overland flow, ephemeral gully, and stream channel areas [28], minus the amount of sediment deposited on such transfer zones and on the valley floodplains. The result is the amount of sediment conveyed downstream to the outlet of the basin. Four environmental factors determine the amount of water erosion and sedimentation. They are climate, soil, topography, and land-use, which operate independently and interactively. Basic characteristics and spatio-temporal features are thus taken into account in a hierarchical structure for discovering erosional phenomenon. In particular, the evolution over time of net erosion reflects the magnitude and frequency of individual storm events, which are nested within larger events occurring on different time scales [21].

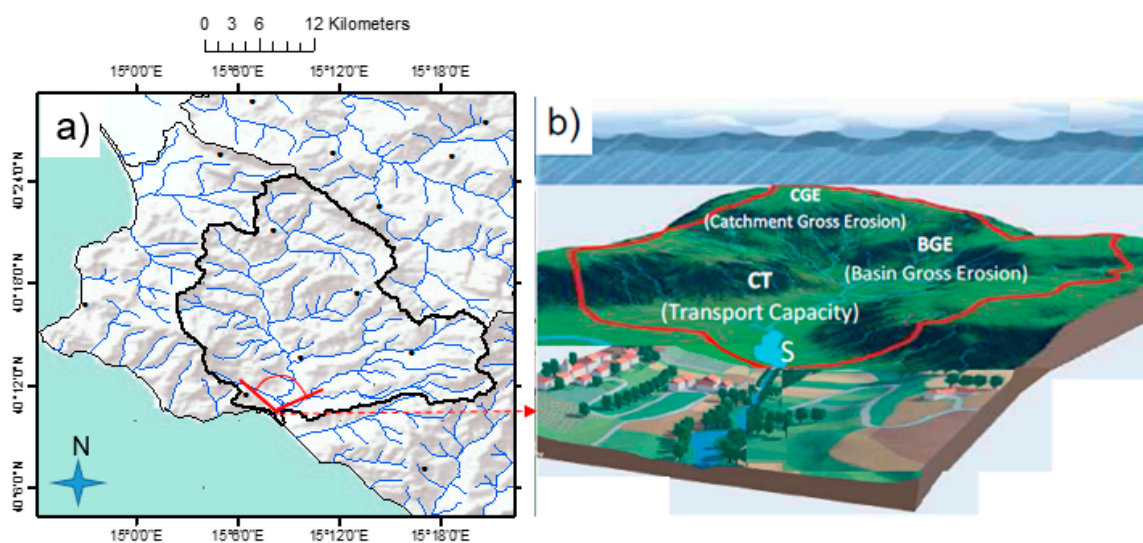


Figure 3. (a) Orography of the ARB with the fluvial drainage network facing the Tyrrhenian Sea and (b) three-dimensional (3-D) exemplary view of landscape hydro-geomorphological processes in a nested scheme for the ARB.

Figure 3b outlines the role played in sediment transport by mesoscale rainstorms accounted at the basin scale (BGE, basin gross erosion), while also assuming that the distribution of local showers play an important role in determining torrential flows rich in sediment in the individual river catchments of the basin (CGE, catchment gross erosion).

The model structure suggests that spring–summer (May to September) precipitation is an important factor to estimate the relative contribution of individual catchments (upper tributaries river) to the sediment (CGE) moving within the basin drainage system. In contrast, winter precipitation mostly contributes to basin-wide transient response (BGE within lower tributary river).

Since the procedure for determining rainfall erosivity suggested by Wischmeier and Smith [36] is applicable to the computation of annual erosion, its use to estimate soil loss from single storms would imply considerable errors [37] and motivate a reinterpretation of the original formulation. Foster et al. [30] and Thornes [31] elaborated the concept of the balance between driving and resisting forces in sediment budget. We further arranged this solution to model net erosion on a monthly basis (NETAM, $\text{Mg km}^{-2} \text{ month}^{-1}$) as:

$$NETAM = A \cdot \left[k \cdot S^n \left(\alpha \cdot R_S^u + \beta \cdot R_Q^m \right) \cdot e^{-\nu \cdot VCF} \right] \quad (1)$$

where the term within round brackets is the modified Foster algorithm; R_S is the rainfall-erosivity indicator associated with splash erosion; R_Q (mm) is the runoff term, associated with transport erosion;

S (m^{-1}) is the mean slope of the basin; the erodibility coefficient (lithology factor) $k = 0.0145$ and the shape parameters (which play an adjusting role on the model inputs) $n = 2$ and $m = 2$ were arranged from Wainwright and Mulligan [11], and u was determined by calibration; $\exp(-\nu \cdot VCF)$, with $\nu = 0.07$, is the exponential vegetation function [31], with VCF (%) being the vegetation cover fraction [16]; A and α are erosivity scale coefficients, whose values were determined by calibration.

Our approximation is that hydraulically rough and vegetated surfaces reduce flow velocity and, hence, soil interrill transport capacity [28]. This is reflected in the low values attributed to parameters k and ν in Equation (1). Then, as canopy cover reduces soil detachment caused by raindrop impact, it also reduces interrill sediment transport capacity by attenuating raindrop impact. Based on this understanding, the power of rainfall as prevailing storm erosivity in summer and autumn is captured by the daily rainfall term of R_S , while in winter and spring, runoff is captured by the monthly rainfall terms of R_Q . In the ARB, predominant water erosion derives from interactions between the detachment on hillslope areas caused by water drops falling on soil, and successive runoff towards downslope up to flow in the drainage networks. This linkage of processes occurs within a fluctuating and continuous interplay of disturbing and resistance forces. In this way, soil erosion by water mostly occurs when the detachment of particles and their subsequent transportation experience a greater driving force than the force binding particles into the vegetated slope. With all these processes, rainfall is used by nature as both a driving and a resisting factor. To better detail this, firstly the erosive influence of rainfall increases with water amount, intensity, and runoff; secondly, and opposing this influence, the protective effect of vegetation increases with precipitation amount.

To further explain the single terms of Equation (1), arranging from Diodato and Aronica [38], we obtain:

$$R_S = \sqrt{dx} \cdot (dx \cdot f(jm)) \quad (2)$$

where dx is the daily maximum rainfall (mm) in each j month; the scale-factor $f(jm)$ is as follows:

$$f(jm) = \left(1 - 0.45 \cdot \cos\left(6.28 \frac{j - 2.5}{22 - j} \right) \right) \quad (3)$$

The semi-parametric function $f(jm)$ modulates the intra-seasonal storm intensity proxy during rainfalls.

The following R_Q term represents, instead, the erosivity mostly associated with runoff erosion:

$$R_Q = (p + p_{j-1}) \cdot w \quad (4)$$

where p is the amount of rainfall (mm) in the current month and p_{j-1} (mm) is the rainfall in the previous month; w is an indicator of soil humidity, in the form of a semi-parametric function, to modulate the intra-seasonal humidity after precipitation:

$$w = \left(0.5 + 0.4 \cdot \cos\left(6.28 \frac{j + 0.5}{24 - j} \right) \right) \quad (5)$$

4. Results and Discussion

Overall results of the calibrated model (1951–1990) and sub-model (rainfall erosivity and runoff) validation are first presented, followed by the model-based reconstruction of net erosion data for the period 1951–2018. The long-term trend is discussed at the annual scale, before highlighting the net erosion variability at the monthly scale.

4.1. Model Calibration

For the calibration period 1951–1990, over which long-term annual mean of net erosion data was available for the ARB, the values of the coefficients $u = 2$, $A = 1500$ (which converts values of eroded

soil from mm to Mg km^{-2} , and $\alpha = 0.1$ in Equation (1) were obtained by approximating the model output to the silting value determined experimentally from the degree of filling of the dam of Piano della Rocca ($490 \text{ Mg km}^{-2} \text{ year}^{-1}$), covering 24% of the entire basin [34]. If the figure of $490 \text{ Mg km}^{-2} \text{ year}^{-1}$ for the period 1951–1990 is extrapolated for the whole of the basin, then the overall erosion rate calculates to $2042 \text{ Mg km}^{-2} \text{ year}^{-1}$. The calibrated estimate was $2041 \text{ Mg km}^{-2} \text{ year}^{-1}$ for the same period.

4.2. Semi-Quantitative Validation

To ensure that the model serves its intended purpose, a semi-quantitative verification with inter-monthly variability was done, since sub-models of Equations (2) and (4) do not include any scale parameter. Figure 4 shows the performance of these sub-models. In particular, Figure 4a displays that the rainfall-erosivity component is in agreement with RUSLE-based erosivity data [35]. Figure 4b also reflects a satisfactory performance between predicted and actual runoff data [33].

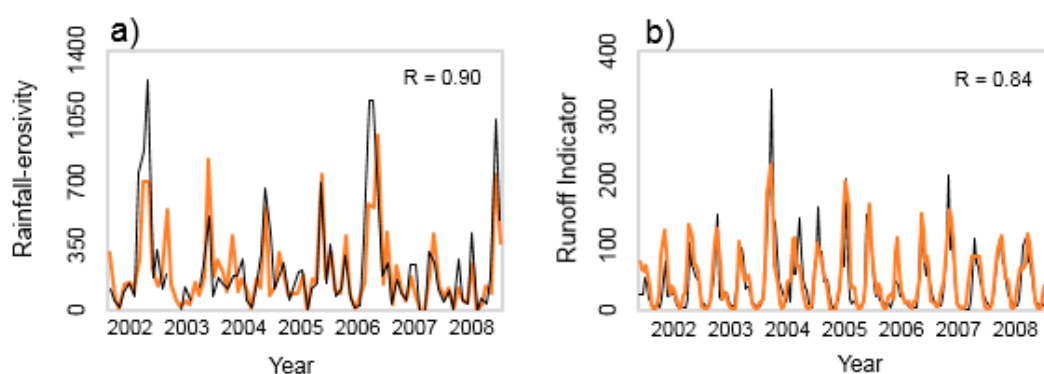


Figure 4. (a) Predicted erosivity indicator (orange curve, Equation (2)) and actual rainfall-erosivity (black curve, $\text{MJ mm ha}^{-1} \text{ h}^{-1} \text{ month}^{-1}$) for Gioi Cilento station (2002–2008), and (b) predicted runoff indicator (orange curve, Equation (4)) and actual runoff in mm (black curve) for the ARB (1958–1972).

This indicates that, at basin scale, net erosion is not the result of the runoff amount only, but of the combination of rainfall erosivity by both raindrop impact and surface runoff. As well, vegetation covers the soil during several months, over which erosion patterns may change [39].

In Figure 5, the model appears to correctly compute the main effects and trends associated with sediment yield, represented in this case by the sand extracted every year (proxy of the net erosion) in the Alento valley [40]. We evaluated the relative performance of the NETAM, without comparing the absolute estimates. Coevolution between material extracted at the valley of ARB (histogram) and simulated net erosion (blue curve) illustrates a substantial agreement, with the only exception of around 1985 (corresponding to the beginning of the construction of the dam in 1984 [34]).

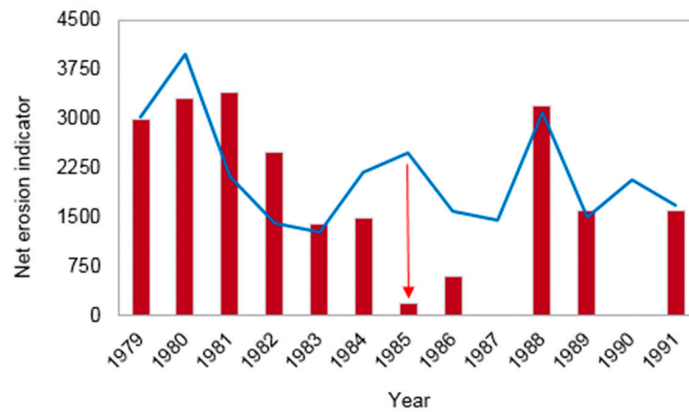


Figure 5. Coevolution time-series of extracted sediment in the Alento valley (histogram) and annual net erosion (blue curve, Equation (1), $\text{Mg km}^{-2} \text{ year}^{-1}$) for the period 1979–1991. Red arrow indicates the disagreement occurring at the start of the dam construction.

4.3. Annual Net Erosion Reconstruction

Figure 6 shows the temporal evolution of annual sediment exports from ARB during the period 1951–2018, as calculated with Equation (1). Part of the estimated sediment was trapped by the dam built in 1994. However, no refinement was brought to the original dataset, as the sediment trapped in the reservoir is still the effective erosion that occurred from the several catchments composing the basin.

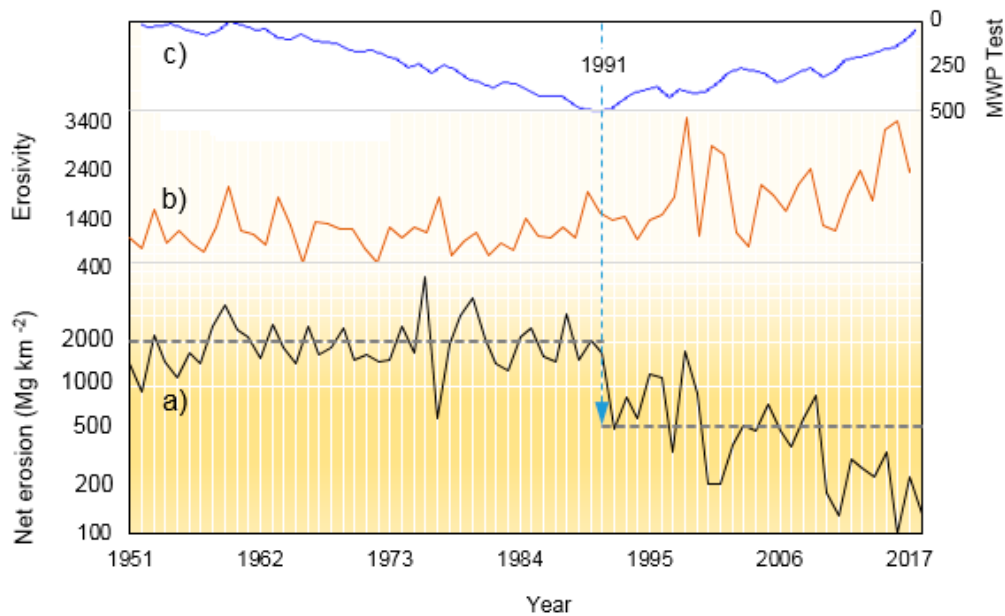


Figure 6. (a) Temporal evolution of the modeled—Equation (1)—annual amount of net erosion over the period 1951–2018 in the ARB (black curve), with the respective long-term mean values (bold dashed grey lines) before and after the change-point of 1991 (vertical dashed blue line). (b) Rainfall-erosivity in $\text{MJ mm ha}^{-1} \text{ h}^{-1} \text{ year}^{-1}$ (orange curve) and (c) Mann-Whitney-Pettitt (MWP) test (blue curve) for the change-point detection.

Figure 6a, in particular, shows the actual evolution of net erosion that, after the first years with low erosional rate, reveals an increase from 1960 at a roughly constant trend that extended until 1990, before the change-point detected in 1991 (Figure 6c) with the Mann-Whitney-Pettitt test [41]. After this year, the sediment rate underwent a continuous irregular decrease until the end of the time-series.

Over the first period, 1951–1990, the average estimated net erosion value is of $2041 \text{ Mg km}^{-2} \text{ year}^{-1}$ ($\pm 889 \text{ Mg km}^{-2} \text{ year}^{-1}$ standard deviation), while in the last period, 1991–2018, the average

value stands at $568 (\pm 436 \text{ Mg km}^{-2} \text{ year}^{-1})$ standard deviation), with a marked decrease of $1473 \text{ Mg km}^{-2} \text{ year}^{-1}$ compared to the previous period. This decrease is also accompanied by an amplification of the interannual variation coefficient of net erosion, which passes from 0.42 for the period before the change-point, to 0.58 for the following period. The growing seasonal irregularity of the precipitation is probably the major driver of the increasing interannual variability of soil erosion. Over 1991–1998, forest cover doubled and cropland roughly halved due to decades of land abandonment and reduction of human pressure [42], and this is likely the cause of decrease in net erosion during the period 1991–2018, although rainfall-erosivity kept on rising (Figure 6b). Thus, vegetation cover exerted a great resistance to the hydrological hazard, since vegetation underwent a general increase after 1990 [16]. However, during the most extremes hydrological events (e.g., precipitation at hours or sub-hourly scales), soil erosion in small catchments could represent a large risk for soil mobilization and transport, which can contribute to nutrient and organic carbon losses.

4.4. Net Erosion Monthly Variability and Timing

The use of monthly data helps summing up consecutive hydro-geomorphological events over an appropriate time scale, with respect to hydrological timing and crop growing cycles or scheduling of tillage practices. The modeled results, obtained over 68 years, show that there is a significant variation of sediment transport at the intra-seasonal scale in both past (1951–1990) (Figure 7a) and recent (1991–2018) periods (Figure 7b, grey bars). Almost half of suspended solid transport occurs in autumn (43% and 54%, respectively, in the two periods) and approximately one third of the annual flux occurs in winter (39% and 29%, respectively). However, the 95th percentile (Figure 7, empty bars) is distributed differently than to mean values, with more divergence in April and September (Figure 7, red bars). This divergence represents a high risk of soil erosion in correspondence to the months with tilled soil in both the periods, although results evidence a decrease of net erosion in all months during the recent phase 1991–2018 (Figure 7b).

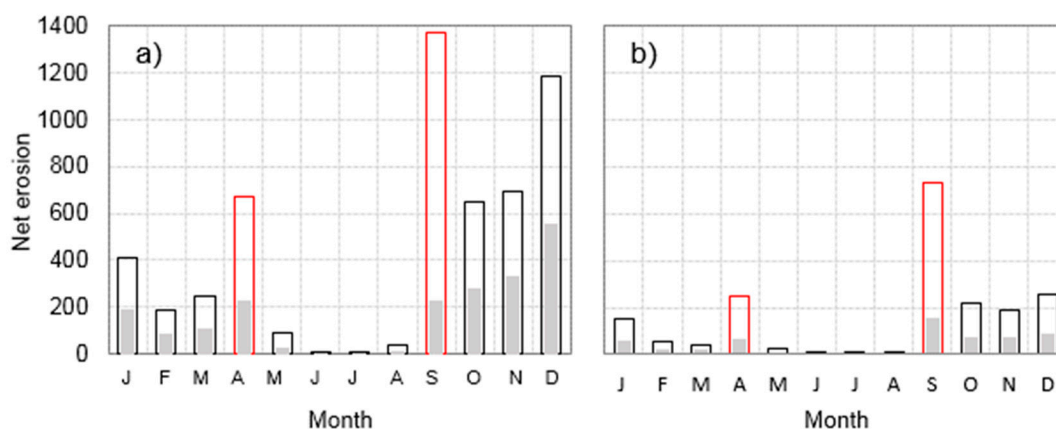


Figure 7. Seasonal evolution of modeled—Equation (1)—net erosion with mean values (grey bars) and 95th percentile (empty bars) during (a) 1951–1991 and (b) 1991–2018 for the ARB (in red bars, the erosional soil degradation hazard in April and September months, when storms occur with tilled soil).

The autumn season seems to maintain the primacy of erosion rates, in past as in recent times. Rizzi [43] documented disasters in the Alento coast in autumn and winter during past times.

In winter, rainfall and average sediment are significant, but most of the erodible particles are transported by the first floods of the preceding autumn. Spatial timeline of storminess also shows a decadal trend (Figure 8). The increasing trend has affected practically the entire basin, especially for storms of 24-h duration (Figure 8b). Then, the increased variability and amount of storms found at the Gioi Cilento station can affect the areas around the station. In particular, it is understood that an average increase of 10 mm per half a century affected the storms of 1-h duration (Figure 8a), and 10–20 mm the

storms of 24-h duration (Figure 8b). The areas of the basin more interested from storm increases are those included along the transect zone around the villages of Cicerale (40°21' N, 15°08' E), Gioi Cilento (40°17' N, 15°13' E), and Vallo della Lucania (40°14' N, 15°16' E).

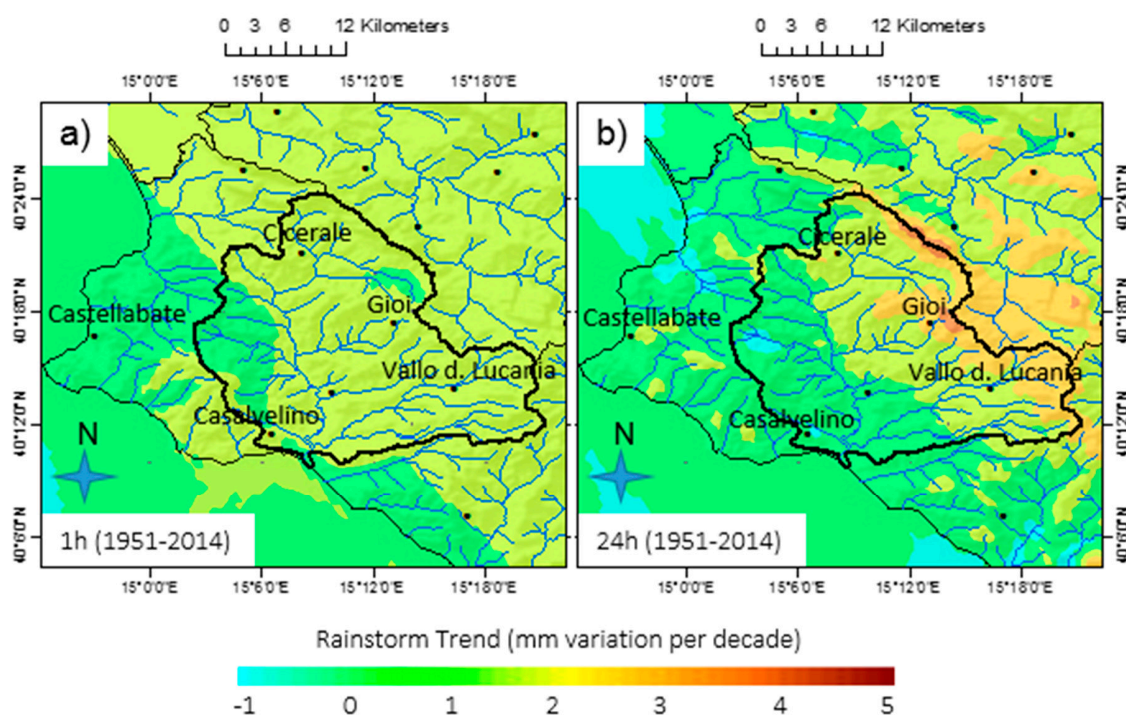


Figure 8. (a) 1-h duration rainstorm trend (mm decade^{-1}) and (b) as in (a) for 24-h rainstorm durations during the period 1951–2014 across the ARB (arranged from ESRI-Geostatistical Analysis via de-trended ordinary cokriging using as covariate the elevation).

5. Conclusions

Land use change has been recognized throughout the world as an important driver of climate-driven geomorphological processes, which may also trigger changes in carbon cycling [44]. Soil erosion rates may be expected to change in response to changes in climate and vegetation for a variety of reasons, the most direct of which is the change in the erosive power of rainfall and resistance forces, respectively. However, modeling rainfall-driven soil erosion rates is difficult because of the lack of long-term data in river basins. In particular, complex models are often not adequate to reconstruct net erosion (or sediment yield) changes because they require a considerable amount of high-resolution input data, not always available on long timescales. Thus, the use of parsimonious models offers an interesting possibility to reconstruct net erosion series on a monthly basis. This is what we have done with the NETAM, developed on the original Foster and Thornes algorithms, in a test site, the Alento River Basin ($\sim 400 \text{ km}^2$ in Southern Italy). Though the model developed for the ARB is not easily transferable for applications in other basins, it provided a peculiar and unique opportunity for modeling erosion responses to climate and land cover changes, where documented hydrological processes at basin scale also support input-data generation and interpretation of results. The ARB is a catchment with extensive natural areas. The development of agricultural and natural areas is favored by the presence of farming practices and a markedly seasonal climate. Thanks to the continuous observation of selected physical environmental variables, we were able to establish seasonal patterns of weathering processes and identify the factors that control rainfall erosivity and runoff and, in turn, net erosion. Cold and wet cycles in winter and wet and dry cycles in spring–autumn are the main processes involved in landscape weathering, thereby controlling slope development together with rainfall-related erosion processes. The main observed feature is the reaction of the ARB to all rainfall

events. Hydrological events show high fluctuations of the suspended sediment by month-to-month, and by year-to-year, deriving from a heterogeneous temporal distribution related to seasonal variations of the hydro-climatic forcing (that is, surface erosivity and runoff) and the vegetation cover. In this way, NETAM values were obtained for the period 1951–2018 by using parsimonious erosion sub-models and land cover statistics from documented agrarian sources. We conclude that if pulses of sediment fluctuation in the ARB have always been driven mainly by natural climatic oscillations, then land abandonment and revegetation are the causes of the observed reduction of net soil erosion in the last decades. This study adds to a growing body of literature on the development of methodological frameworks and tools that could be used to outline scenarios of soil erosion and instability risks resulting from climate changes (e.g., increasing heavy rainfall events), and changes in land use and management practices in central Italy [45–47].

Author Contributions: N.D. conceived the study, performed the analysis, and drafted the manuscript. G.B. contributed to the analysis and wrote the final manuscript.

Funding: This is an investigator-driven study without any grant support.

Acknowledgments: We acknowledge the support of Mauro Biafore, Director of Centro Funzionale Multirischi Protezione Civile della Regione Campania (Naples, Italy), and Matteo Gentilella of the same center, who provided the rainfall data used in this study.

Conflicts of Interest: The authors declare no conflicts of interest.

References

- Jentsch, A.; Beierkuhnlein, C. Research frontiers in climate change: Effects of extreme meteorological events on ecosystems. *Comptes Rendus Geosci.* **2008**, *340*, 621–628. [[CrossRef](#)]
- Li, Z.; Fang, H. Impacts of climate change on water erosion: A review. *Earth-Sci. Rev.* **2016**, *163*, 94–117. [[CrossRef](#)]
- Riebau, A.R.; Fox, D.G. Damage Assessment of Agrometeorological Relevance from Natural Disasters: Economic and Social Consequences. In *Natural Disasters and Extreme Events in Agriculture*; Springer Science and Business Media LLC: Berlin/Heidelberg, Germany, 2005; pp. 119–135.
- Yin, J.; Gentine, P.; Zhou, S.; Sullivan, S.C.; Wang, R.; Zhang, Y.; Guo, S. Large increase in global storm runoff extremes driven by climate and anthropogenic changes. *Nat. Commun.* **2018**, *9*, 4389. [[CrossRef](#)] [[PubMed](#)]
- Blaschke, P.M.; Trustrum, N.A.; Hicks, D.L. Impacts of mass movement erosion on land productivity: A review. *Prog. Phys. Geogr. Earth Environ.* **2000**, *24*, 21–52. [[CrossRef](#)]
- Leeder, M.R.; Harris, T.; Kirkby, M.J. Sediment supply and climate change: Implications for basin stratigraphy. *Basin Res.* **1998**, *10*, 7–18. [[CrossRef](#)]
- Coulthard, T.J.; Kirkby, M.J.; Macklin, M.G. Modelling geomorphic response to environmental change in an upland catchment. *Hydrol. Process.* **2000**, *14*, 2031–2045. [[CrossRef](#)]
- Higgitt, D.L. A brief time of history. In *Geomorphological Processes and Landscape Change: Britain in the Last 1000 Years*; Higgitt, D.L., Lee, E.M., Eds.; Blackwell Publishers Ltd.: Oxford, UK, 2001; pp. 1–26.
- Verstraeten, G.; Poesen, J. Factors controlling sediment yield from small intensively cultivated catchment in a temperate humidclimate. *Geomorphology* **2001**, *40*, 123–144. [[CrossRef](#)]
- Trimble, S.W.; Crosson, P.U.S. Soil erosion rates—Myth and reality. *Science* **2000**, *289*, 248–250. [[CrossRef](#)]
- Wainwright, J.; Mulligan, M. *Environmental Modelling: Finding Simplicity in Complexity*; John Wiley and Sons, Ltd.: Chichester, UK, 2004; p. 408.
- Pelletier, J.D. A spatially distributed model for the long-term suspended sediment discharge and delivery ratio of drainage basins. *J. Geophys. Res. Space Phys.* **2012**, *117*, 02028. [[CrossRef](#)]
- Syvitski, J.P.M.; Milliman, J.D. Geology, Geography, and Humans Battle for Dominance over the Delivery of Fluvial Sediment to the Coastal Ocean. *J. Geol.* **2007**, *115*, 1–19. [[CrossRef](#)]
- Kettner, A.J.; Restrepo, J.D.; Syvitski, J.P.M. A Spatial Simulation Experiment to Replicate Fluvial Sediment Fluxes within the Magdalena River Basin, Colombia. *J. Geol.* **2010**, *118*, 363–379. [[CrossRef](#)]
- Budetta, P. Landslide hazard assessment of the Cilento rocky coasts (Southern Italy). *Int. J. Geol.* **2013**, *7*, 1–8.

16. Romano, N.; Nasta, P.; Bogena, H.; De Vita, P.; Stellato, L.; Vereecken, H. Monitoring Hydrological Processes for Land and Water Resources Management in a Mediterranean Ecosystem: The Alento River Catchment Observatory. *Vadose Zone J.* **2018**, *17*, 1–12. [[CrossRef](#)]
17. Shrestha, D.; Zinck, J.; Van Ranst, E. Modelling land degradation in the Nepalese Himalaya. *Catena* **2004**, *57*, 135–156. [[CrossRef](#)]
18. Renschler, C.S.; Harbor, J.; Harbor, J. Soil erosion assessment tools from point to regional scales—the role of geomorphologists in land management research and implementation. *Geomorphology* **2002**, *47*, 189–209. [[CrossRef](#)]
19. Ramos, M.C.; Mulligan, M. Impacts of climate variability and extreme events on soil hydrological processes. In Proceedings of the EGS-AGU-EUG Joint Assembly, Nice, France, 6–11 April 2003. Abstract id. 11592.
20. Alexandrov, V.A. Vulnerability of agronomic systems in Bulgaria. *Clim. Chang.* **1997**, *36*, 135–149. [[CrossRef](#)]
21. Thomas, M.F. Landscape sensitivity in time and space—An introduction. *Catena* **2001**, *42*, 83–98. [[CrossRef](#)]
22. Reinhard, M.; Alexakis, E.; Rebetz, M.; Schlaepfer, R. Climate-soil-vegetation interactions: A case study from the forest fire phenomenon in Southern. In Proceedings of the EGS-AGU-EUG Joint Assembly, Nice, France, 6–11 April 2003. Abstract id. 2470.
23. Krishnaswamy, J.; LaVine, M.; Richter, D.D.; Korfmacher, K. Dynamic modeling of long-term sedimentation in the Yadkin River basin. *Adv. Water Resour.* **2000**, *23*, 881–892. [[CrossRef](#)]
24. Nearing, M.A.; Jetten, V.; Baffaut, C.; Cerdan, O.; Couturier, A.; Hernández, M.; Le Bissonnais, Y.; Nichols, M.H.; Nunes, J.P.; Renschler, C.S.; et al. Modeling Response of Soil Erosion and Runoff to Changes in Precipitation and Cover. *Impacts Glob. Clim. Chang.* **2005**, *61*, 1–11.
25. Pruski, F.F.; Nearing, M.A. Climate-induced changes in erosion during the 21st century for eight U.S. locations. *Water Resour. Res.* **2002**, *38*, 34-1–34-11. [[CrossRef](#)]
26. Cohen, S.; Kettner, A.J.; Syvitski, J.P. Global suspended sediment and water discharge dynamics between 1960 and 2010: Continental trends and intra-basin sensitivity. *Glob. Planet. Chang.* **2014**, *115*, 44–58. [[CrossRef](#)]
27. De Vente, J.; Poesen, J.; Verstraeten, G. The application of semi-quantitative methods and reservoir sedimentation rates for the prediction of basin sediment yield in Spain. *J. Hydrol.* **2005**, *305*, 63–86. [[CrossRef](#)]
28. Toy, T.J.; Foster, G.R.; Renard, K.G. *Soil Erosion: Prediction, Measurement, and Control*; John Wiley & Sons, Inc.: New York, NY, USA, 2002; p. 338.
29. Tarboton, D.; Pack, R.T.; Luce, C.H.; Istanbuluoglu, E. Modeling of the interactions between forest vegetation, disturbances, and sediment yields. *J. Geophys. Res. Space Phys.* **2004**, *109*, 01009.
30. Foster, G.R.; Meyer, L.D.; Onstad, C.A. A Runoff Erosivity Factor and Variable Slope Length Exponents for Soil Loss Estimates. *Trans. ASAE* **1977**, *20*, 683–687. [[CrossRef](#)]
31. Thornes, J.B. The interaction of erosional and vegetational dynamics in land degradation: Spatial outcomes. In *Vegetation and Erosion: Processes and Environments*; Thornes, J.B., Ed.; John Wiley & Sons: Chichester, UK, 1990; pp. 45–55.
32. Lapenna, M.R.; Rosati, L.; Salerno, G.; Villani, M.; Fascetti, S.; Filesi, L. Landscape planning and biodiversity conservation of river habitats require vegetation analysis and mapping: The case of Cilento National Park (Italy). In *Latest Trends in Energy, Proceedings of the 7th International Conference on Environmental and Geological Science and Engineering (EG '14); Proceedings of the 7th International Conference on Urban Planning and Transportation (IPT '14); Proceedings of the 3rd International Conference on Energy Systems, Environment, Entrepreneurship and Innovation (ICESEEI '14) Environment and Development, Salerno, Italy, 3–5 June 2014*; Griselda, J., Breton, C., Quartieri, J., Guida, M., Guida, D., Guarnaccia, C., Eds.; WSEAS: Sofia, Bulgaria, 2014; pp. 182–190.
33. SIMN. *Hydrological Annals*; Servizio Idrografico e Mareografico Nazionale: Rome, Italy, 1957–1972. (In Italian)
34. De Vita, P.; La Barbera, G. Studi per il progetto di gestione dell'invaso di Piano della Rocca sul fiume Alento (Campania Meridionale): Qualità delle acque e stima dell'interrimento. In Proceedings of the Atti del XXX Convegno di Idraulica e Costruzioni Idrauliche IDRA, Rome, Italy, 10–15 September 2006; pp. 1–16. (In Italian).
35. Chirico, G.B.; De Falco, M.; Diodato, N.; Romano, N.; Santini, A. Estimating rainfall erosivity from daily precipitation records in Campania region (Southern Italy). In Proceedings of the EGU General Assembly 2010, Vienna, Austria, 2–7 May 2010; p. 7084.

36. Wischmeier, W.H.; Smith, D.D. *Predicting Rainfall Erosion Losses from Cropland East of the Rocky Mountains: Guide for Selection of Practices for Soil and Water Conservation, Issues 282–290*; Agricultural Handbook 282; U.S. Department of Agriculture: Brooksville, FL, USA, 1965; p. 47.
37. Haan, C.T.; Barfield, B.J.; Hayes, J.C. *Design Hydrology and Sedimentology for Small Catchments*; Academic Press: San Diego, CA, USA, 1994; p. 588.
38. Diodato, N.; Aronica, G. Finding simplicity in storm erosivity modelling. In *Storminess and Environmental Change: Climate Forcing and Response in the Mediterranean Region*; Diodato, N., Bellocchi, G., Eds.; Springer: Dordrecht, The Netherlands, 2014; pp. 53–64.
39. Kirkby, M.; Abrahart, R.; McMahon, M.; Shao, J.; Thornes, J. MEDALUS soil erosion models for global change. *Geomorphology* **1998**, *24*, 35–49. [[CrossRef](#)]
40. Aloia, A.; Maietta, S.; Moretta, F.; Romano, E.; Mugnani, M.; Positano, M.P.; Tedesco, A.; Banco, C.; Andreola, V.; Liguori, V.; et al. *Progetto di Piano Stralcio Erosione Costiera*; Ai sensi dell'art. 17 commi 1 e 6 della Legge 18 maggio 1989 n. 183 s.m.i. e Legge 4 dicembre 1993 n. 493; Autorità di Bacino Regionale Sinistra Sele: Salerno, Italy, 2005; p. 29. (In Italian)
41. Pettitt, A.N. A non-parametric approach to the change-point detection. *Appl. Stat.* **1979**, *28*, 126–135. [[CrossRef](#)]
42. Nasta, P.; Palladino, M.; Ursino, N.; Saracino, A.; Sommella, A.; Romano, N. Assessing long-term impact of land-use change on hydrological ecosystem functions in a Mediterranean upland agro-forestry catchment. *Sci. Total. Environ.* **2017**, *605*, 1070–1082. [[CrossRef](#)]
43. Rizzi, F. *Osservazioni Statistiche Sul Cilento*; Tipografia di Angelo Trani: Naples, Italy, 1809; p. 6. (In Italian)
44. Van Oost, K.; Quine, T.A.; Govers, G.; De Gryze, S.; Six, J.; Harden, J.W.; Ritchie, J.C.; Mccarty, G.W.; Heckrath, G.; Kosmas, C.; et al. The Impact of Agricultural Soil Erosion on the Global Carbon Cycle. *Science* **2007**, *318*, 626–629. [[CrossRef](#)]
45. Borrelli, P.; Modugno, S.; Panagos, P.; Marchetti, M.; Schütt, B.; Montanarella, L. Detection of harvested forest areas in Italy using Landsat imagery. *Appl. Geogr.* **2014**, *48*, 102–111. [[CrossRef](#)]
46. Alvioli, M.; Melillo, M.; Guzzetti, F.; Rossi, M.; Palazzi, E.; Von Hardenberg, J.; Brunetti, M.T.; Peruccacci, S. Implications of climate change on landslide hazard in Central Italy. *Sci. Total. Environ.* **2018**, *630*, 1528–1543. [[CrossRef](#)]
47. Piacentini, T.; Galli, A.; Marsala, V.; Miccadei, E. Analysis of Soil Erosion Induced by Heavy Rainfall: A Case Study from the NE Abruzzo Hills Area in Central Italy. *Water* **2018**, *10*, 1314. [[CrossRef](#)]



© 2019 by the authors. Licensee MDPI, Basel, Switzerland. This article is an open access article distributed under the terms and conditions of the Creative Commons Attribution (CC BY) license (<http://creativecommons.org/licenses/by/4.0/>).